Incompressible Laminar Entry Flows in a Square Duct of Strong Curvature Using an Implicit SMAC Scheme

B. R. Shin*1 and T. Ikohagi*2

SMAC 陰解法에 의한 큰 曲率를 갖는 正四角形 덕트內의 非壓縮性 層流 入口流動

申 炳 錄, 井小萩 利 明

원심형 임펠러 내부 流路등 큰 曲率을 수반하는 터보기계 要素의 유동해석을 위한 계산 코드를 개발하였다. 이 코드에서는 곡선좌표계에 유도된 3차원 비압축성 Navier-Stokes의 운동 방정식을 SMAC 陰解法으로 푼다. 이 코드를 이용하여 유로의 斷面이 정사각형이고 90 度로 굽은 덕트내부의 층류 入口流動을 해석하고, 굽은 管 특유의 유동현상을 수치모사하였다. 또한 曲管部 입구에서 충분히 발달한 유동, 또는 발달중인 유동이 유입될 경우에 이것이 곡관부 내부의 유동에 미치는 영향을 上·下流의 계산영역이 서로 다를 몇몇 유동장에 대하여 조사하고, 본 계산에서 얻어진 결과와 실험결과와의 비교로 본 3차원 유동해석 코드의 有效性을 검토 하였다.

Key Words: Implicit SMAC Scheme(SMAC 음해법), Entry Flow(입구유동), Incompressible Flow(비압축성 유동), Finite Difference Method(유한차분법), Navier-Stokes Equations(Navier-Stokes 방정식), Duct Flow(덕트 유동)

1. Introduction

Flows in curved ducts are encountered in a wide range of practical engineering applications such as blade passage, intake or draft tube of turbomachinery, piping systems of plants, cooling coils of heat exchangers and biomechanical circuits. As compared with simple cross-section of the ducts, such flows induce complex secondary flows within the duct on account of existence of the curvature along the streamwise. These flows can result in large redistributions of the streamwise velocity, a pressure loss and increased heat transfer at the duct wall. From the engineering point of view, it is an important task to understand those flows accurately. As a example, draft tube in hydraulic turbine, which has a role to reduce the velocity and increase the pressure of the water discharging, could have an important effect on the efficiency of the turbine, so better understanding of the flow behavior in the tube is highly required. For these reasons, many studies to analyze the curved duct flows have been made by experiments[1-2] and computations[3-4]. In many types of curved ducts, the 90-degree bended square duct is the most proper fluid dynamic devices[5] to understand complex flow phenomena in a three-dimensional (3-D) curved passage.

*1. Member, Institute of Fluid Science, Tohoku University, Sendai 980-77, Japan
*2. Institute of Fluid Science, Tohoku University, Sendai 980-77, Japan

Recently as technologies advance, the gravity of studying numerical schemes to simulate practical flows is high because better performance, compact and highly efficient designs are required in modern flow devices. Among numerical methods, the most widely used ones for computing the incompressible flow are the MAC type schemes and the pseudo-compressibility methods. The MAC type schemes[6-8] are an epoch-making method in which the continuity condition is satisfied identically and the spurious error, that is checkerboard like oscillation of pressure, is removed completely by introducing a staggered grid. On the other hand, the pseudo-compressibility method[9-10] has been used only for the steady state flow. Because, while the incompressible flow has an elliptic character, the pseudo-compressibility method based on the compressible flow scheme has a hyperbolic character, so the disturbance spreads just inside a limited region. However, recently this method has been extended to the unsteady flow by Kwak et al.[11]. The authors have already proposed some implicit SMAC schemes and applied to laminar and turbulent flow problems[12-13]. In these schemes, a staggered grid in curvilinear coordinates is applied, and the elliptic equation of pressure is solved by using the vectorized Tschebyscheff SLOR method. Therefore, the elliptic character of incompressible flow is satisfied well.

The purpose of this paper is to develop an efficient computer code for solving the passage flow of turbomachinery with very complicated flow fields, and understand complex flow phenomena in a strongly curved duct which is to be basic physical elements associated with above mentioned practical fluid devices. In this paper, a numerical study of laminar flow phenomena in a 90-degree bend is performed using implicit SMAC scheme[12]. In the present study, the geometry of the curved area is the same as that of Humphrey et al.[2]. Detailed observations of the secondary flows and the redistribution of the streamwise velocity obtained at the different entry flows and different up- and downstream boundary positions are made. Also, comparisons of present predicted results with available experimental data are provided.

2. Fundamental Equations

2.1 Fundamental Equations in Curvilinear Coordinates

The fundamental equations of the incompressible flow are the Navier-Stokes equations and the continuity equation expressed in the conservative vector forms

$$\frac{\partial \boldsymbol{u}}{\partial t} + \nabla \cdot \boldsymbol{u}\boldsymbol{u} = -\nabla p + \nu \nabla^2 \boldsymbol{u} \tag{1}$$

$$\nabla \cdot \boldsymbol{u} = 0 \tag{2}$$

where $\boldsymbol{u}$, p and ν are the velocity, static pressure and kinematic viscosity, respectively. Here these equations are extended to the 3-D curvilinear coordinates and applied to the implicit formulation in order to improve the computational efficiency.

Introducing the contravariant velocities U_i and the contravariant vorticities Z_i, the 3-D incompressible momentum equations of the volume fluxes JU_ℓ in general curvilinear coordinates can be derived from Eqs.(1) and (2) as follows:

$$\frac{\partial}{\partial t}(JU_\ell) + L(JU_\ell, p) = 0 \quad (\ell = 1,2,3) \tag{3}$$

$$\frac{\partial}{\partial \xi_i}(JU_i) = 0 \tag{4}$$

where,

$$L(JU_\ell, p) \equiv \frac{\partial}{\partial \xi_i}(JU_i U_\ell) - JU_i \boldsymbol{u} \cdot \frac{\partial}{\partial \xi_i}\nabla \xi_\ell + \tilde{g}_{\ell i}\frac{\partial p}{\partial \xi_i} + \nu \epsilon_{\ell i j}\frac{\partial}{\partial \xi_i} h_{jk} Z_k, \tag{5}$$

$\tilde{g}_{ij} = Jg_{ij}$, and $\epsilon_{\ell ij}$ is the permutation tensor. The Jacobian J and the metrics g_{ij} and h_{ij} of the transformation from Cartesian coordinates x_i to general curvilinear coordinates ξ_i are $J = \partial(x,y,z)/\partial(\xi,\eta,\zeta)$, $g_{ij} = \nabla\xi_i \cdot \nabla\xi_j$ and $h_{ij} = \partial x_k/\partial\xi_i \cdot \partial x_k/\partial\xi_j$, respectively. And the relations between the physical velocity u_i in x_i space and the contravariant velocity U_i in ξ_i space are $U_i = (\partial\xi_i/\partial x_j)u_j$ and $u_i = (\partial x_i/\partial\xi_j)U_j$ using the summation convention. Similarly the contravariant vorticity Z_i and physical vorticity ζ_i are defined as $Z_i = (\partial\xi_i/\partial x_j)\zeta_j$ and $\zeta_i = \nabla\times\boldsymbol{u} = (\partial x_i/\partial\xi_j)Z_j$.

In Eq.(3), the momentum equations of volume fluxes JU_i correspond to the equations of flows through the each cell sides. Therefore, for the usual body fitted curvilinear coordinate grid, the boundary condition can be imposed very easily. In addition, while the contravariant velocity U_i depends on the grid, the volume fluxes JU_i are independent on the grid spacing in the ξ_i-direction because JU, for example, as a ξ component written as $JU = J\boldsymbol{u}\cdot\nabla\xi = \boldsymbol{u}\cdot\boldsymbol{x}_\eta \times \boldsymbol{x}_\zeta$, is meaning the flow rate through $\xi = const$ cell side divided by the cell side area.

2.2 SMAC Schemes

The dependent variables of fundamental equations are $\boldsymbol{u}$ and p, and the advanced value of $\boldsymbol{u}$ can be determined from the Cauchy problem of Eq.(1). However, the remaining variable p can not determined from the remaining Eq.(2). Taking the divergence of Eq.(1) and using Eq.(2), we can derive the Poisson equation of pressure $\nabla^2 p = -\nabla\cdot(\nabla\cdot\boldsymbol{uu})$. Therefore, the values of p is determined from the boundary value problem. However, the value of $\boldsymbol{u}$ determined in this way does not generally satisfy the continuity condition (2). The MAC scheme[6] and the simplified MAC (SMAC) scheme[7] are those which completely solved this difficulty.

Here, the fundamental equations of the SMAC scheme for Eqs.(3) and (4) can be written as

$$JU_\ell^* = JU_\ell^n - \Delta t L(JU_\ell, p)^n \tag{6}$$

$$\frac{\partial}{\partial\xi_\ell}\left(\tilde{g}_{\ell i}\frac{\partial\phi}{\partial\xi_i}\right) = \frac{1}{\Delta t}\frac{\partial}{\partial\xi_\ell}(JU_\ell^*) \tag{7}$$

$$JU_\ell^{n+1} = JU_\ell^* - \Delta t\tilde{g}_{\ell i}\frac{\partial\phi}{\partial\xi_i} \tag{8}$$

$$p^{n+1} = p^n + \phi \tag{9}$$

where ϕ and the asterisk * denotes the pressure correction and the intermediate time level, respectively. In this scheme, the Navier-Stokes equations Eq.(3) is divided into Eqs.(6) and (8) applying the time-splitting method in which the fully implicit scheme is used to the pressure term. The Poisson equation (7) of the pressure increment ϕ is derived by taking a divergence of Eq.(8) and using the continuity condition $\frac{\partial}{\partial\xi_i}(JU_i)^{n+1} = 0$. Therefore, the advanced value JU_i^{n+1} calculated in this way is satisfied with the continuity condition (4). At each cell side centers, the volume flux JU_i must be defined in stead of the physical velocity components of original MAC scheme[6]. And since the principal part of these difference equations of pressure is expressed in compact form, no spurious error occurs in the computation.

3. Numerical Methods

3.1 Implicit SMAC Scheme

Now, Eq.(6) is extend to an implicit form by applying the delta-form approximate-factorization method[14] and partially including the viscous term in the left hand side. Therefore, the momentun equations of the present implicit SMAC

scheme are as follows[12].

$$[1+\Delta t(\frac{\partial}{\partial\xi}U^n-\nu\frac{\partial}{\partial\xi}\tilde{h}_{22}\tilde{h}_{33}\frac{\partial}{\partial\xi})]\cdot$$
$$[1+\Delta t(\frac{\partial}{\partial\eta}V^n-\nu\frac{\partial}{\partial\eta}\tilde{h}_{33}\frac{\partial}{\partial\eta}\tilde{h}_{11})]\cdot$$
$$[1+\Delta t(\frac{\partial}{\partial\zeta}W^n-\nu\frac{\partial}{\partial\zeta}\tilde{h}_{22}\frac{\partial}{\partial\zeta}\tilde{h}_{11})]\Delta JU^* = RHS_1^n \quad (10)$$

$$[1+\Delta t(\frac{\partial}{\partial\xi}U^n-\nu\frac{\partial}{\partial\xi}\tilde{h}_{33}\frac{\partial}{\partial\xi}\tilde{h}_{22})]\cdot$$
$$[1+\Delta t(\frac{\partial}{\partial\eta}V^n-\nu\frac{\partial}{\partial\eta}\tilde{h}_{33}\tilde{h}_{11}\frac{\partial}{\partial\eta})]\cdot$$
$$[1+\Delta t(\frac{\partial}{\partial\zeta}W^n-\nu\frac{\partial}{\partial\zeta}\tilde{h}_{11}\frac{\partial}{\partial\zeta}\tilde{h}_{22})]\Delta JV^* = RHS_2^n \quad (11)$$

$$[1+\Delta t(\frac{\partial}{\partial\xi}U^n-\nu\frac{\partial}{\partial\xi}\tilde{h}_{22}\frac{\partial}{\partial\xi}\tilde{h}_{33})]\cdot$$
$$[1+\Delta t(\frac{\partial}{\partial\eta}V^n-\nu\frac{\partial}{\partial\eta}\tilde{h}_{11}\frac{\partial}{\partial\eta}\tilde{h}_{33})]\cdot$$
$$[1+\Delta t(\frac{\partial}{\partial\zeta}W^n-\nu\frac{\partial}{\partial\zeta}\tilde{h}_{11}\tilde{h}_{22}\frac{\partial}{\partial\zeta})]\Delta JW^* = RHS_3^n \quad (12)$$

where,

$$RHS_\ell = -\Delta t[\frac{\partial}{\partial\xi_i}(JU_iU_\ell)-JU_i\boldsymbol{u}\cdot\frac{\partial}{\partial\xi_i}\nabla\xi + \tilde{g}_{\ell i}\frac{\partial p}{\partial\xi_i}+\nu\epsilon_{\ell ij}\frac{\partial}{\partial\xi_i}(\tilde{h}_{jk}JZ_k)], \quad (13)$$
$$JU_\ell^* = JU_\ell^n + \Delta JU_\ell^*,$$
$$JZ_i = \epsilon_{\ell ij}\frac{\partial}{\partial\xi_i}(\tilde{h}_{jk}JU_k) \quad (j=1,2,3),$$

and $\tilde{h}_{ij}=h_{ij}/J$. This delta formed implicit SMAC scheme satisfies a diagonally dominant condition with the first order upstream difference scheme and is the TVD stable. Also, this implicit SMAC scheme is suitable for vector or vector parallel machine as compared with the HSMAC scheme[15] and the SIMPLE scheme[16] developed toward scalar machine. In addition, JU_ℓ^* is obtained explicitly by the HSMAC scheme and implicitly by the present implicit SMAC scheme with some direct method of systems of linear equation. In the SIMPLE scheme, however, JU_ℓ^* is solved implicitly by some iteration method so that when the second- or higher-order upstream difference scheme is taken, the linear equation no longer satisfies the diagonally dominant condition. Therefore, the under-relaxation is necessary and the number of iteration is increased. Hence, when vector machine is used, the implicit SMAC scheme applied vectorized Tschebyscheff SLOR method to pressure equation is to be more efficient scheme[17] than the HSMAC scheme or the SIMPLE scheme.

Each equation of Eqs.(10)-(12) can be solved by dividing them into three steps, and each step is the problem solving the simultaneous linear equations with tridiagonal matrix by the Gaussian elimination. And the simultaneous linear equations (7) are here solved by the Tschebyscheff SLOR method alternating sweep directions like the ADI method, which is suitable in supercomputing.

3.2 TVD Upwind-Difference Scheme

The second-order central-difference is basically used for the space derivatives. However, for convection term on the left hand side of Eqs.(10)-(12), the first-order upstream-difference scheme is used to reduce the computational efforts and to accelerate the convergency, and for the right hand side, the TVD upwind difference scheme which has remarkable stability in the 3-D computation is applied. Here the TVD monotone scheme is explained using the simple one-dimensional scalar equation as

$$\frac{\partial u}{\partial t}+\frac{\partial f(a,u)}{\partial x}=0 \quad (14)$$

where $a=\partial f/\partial u$ is the characteristic speed. The finite-difference equation of

Eq.(14) can be generally written in the conservation form

$$u_i^{n+1} + \lambda\theta(\hat{f}_{i+1/2} - \hat{f}_{i-1/2})^{n+1} = u_i^n - \lambda(1-\theta)(\hat{f}_{i+1/2} - \hat{f}_{i-1/2})^n \quad (15)$$

where $\lambda = \Delta t/\Delta x$, $0 \le \theta \le 1$, and $\hat{f}$ is the numerical flux function.

The TVD scheme is expressed as a sum of the first-order upstream-difference scheme and correction terms, and then the correction term is modified locally by a limiter in order to stabilize the solution. The numerical flux of the Chakravarthy-Osher TVD upwind difference scheme[18] becomes

$$\begin{aligned}\hat{f}_{i+1/2} &= (f_i + f_{i+1})/2 \\ &\quad -(Df^+_{i+1/2} - Df^-_{i+1/2})/2 \\ &\quad +\frac{1-\kappa}{4}\text{minmod}[Df^+_{i-1/2}, bDf^+_{i+1/2}] \\ &\quad +\frac{1+\kappa}{4}\text{minmod}[Df^+_{i+1/2}, bDf^+_{i-1/2}] \\ &\quad -\frac{1-\kappa}{4}\text{minmod}[Df^-_{i+3/2}, bDf^-_{i+1/2}] \\ &\quad -\frac{1+\kappa}{4}\text{minmod}[Df^-_{i+1/2}, bDf^-_{i+3/2}] \quad (16)\end{aligned}$$

where, $Df^{\pm}_{j+1/2} = a^{\pm}_{i+1/2}\Delta u_{j+1/2}$, $a^{\pm} = (a \pm |a|)/2$, $\Delta u_{j+1/2} = u_{j+1} - u_j$, $-1 \le \kappa \le 1$, and here the minmod function of $\text{minmod}[x, y] = \text{sign}(x)\max[0, \min\{|x|, y\text{sign}(x)\}]$ which controls the slop of flux was used $1 \le b \le (3-\kappa)/(1-\kappa)$. Particularly, if $\kappa = 1/3$, then Eq.(16) becomes the third-order accurate TVD upstream-difference scheme. Also, as b is larger, the region where the limiter function acts becomes narrower.

4. Numerical Results

Some cases of an incompressible developing and fully developed entry flow through a square duct with 90 degree bend are computed by using the present implicit SMAC scheme. The cross section of the bend is square throughout the bend[2]. The Reynolds number based on the inlet mean velocity (U_0) and the entrance width (H) is 790. The mean radius of the bend is 2.3. Figure 1 illustrates the computational geometry, nomenclature, coordinate system, and grid near the bend.

For the boundary conditions, no-slip condition and the Neumann condition for the pressure were implemented on the solid wall boundary. The inlet and outlet

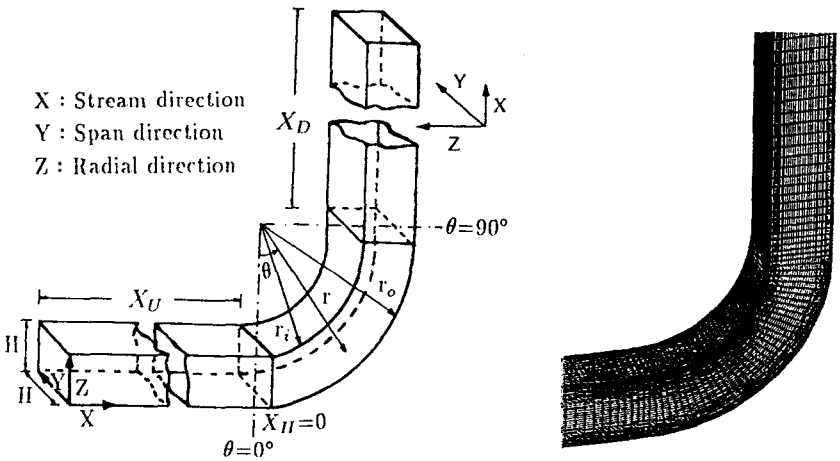

Fig.1 Computational geometry and grid near the bend region

Table 1 Boundary conditions and entrance and exit boundary locations

	Boundary location		Boundary condition		Grid points
	X_U (H)	X_D (H)	Inlet u	Outlet p	$(X\times Y\times Z)$
Case I	5	5	Fully developed flow[19]	Neumann	95×41×41
Case II	7.5	7.5		Dirichlet	107×41×41
Case III	7.5	5	Uniform flow	Dirichlet condition	101×41×41
Case IV	7.5	7.5			107×41×41
Case V	9	5			107×41×41

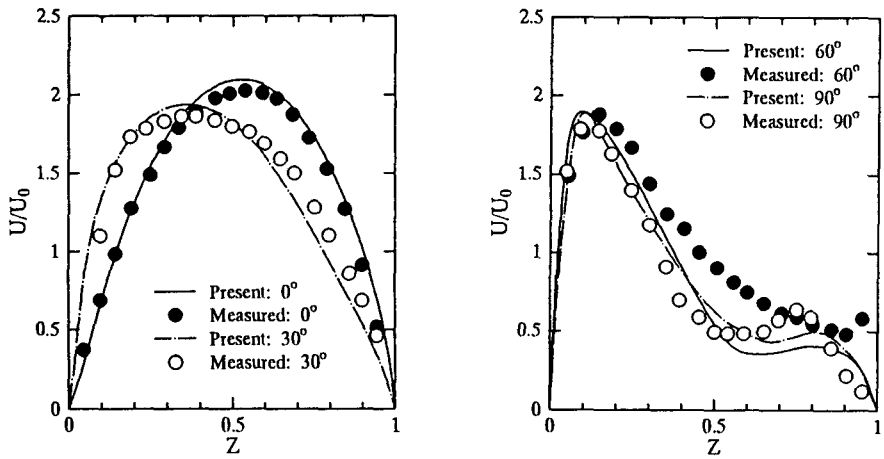

Fig.2 Streamwise velocity profiles at the X-Z symmetry plane (Case I)

boundary conditions, the entrance and exit boundary locations and used grid points for the some computational cases of flow field are shown in Table 1. In the present computation, the control parameter b=4 and κ=1/3 are used in Eq.(16).

In Fig.1 and Table 1, X_U and X_D are represent the length of inlet and outlet boundaries from the bend, respectively. For all cases, the streamwise grid spacing at the bend area is 2.5°.

In the present study, the two results of the fully developed entry flow cases of Case I and II were accorded with each other except the convergency rate of the Case I was somewhat increased. For the developing entry flow cases of the Case III and IV, both results are also the same in spite of the different exit boundary locations. However, the Case V was closer to experimental data[5] than the results of the Case III and IV as it will be shown later in Figs 6 and 7. The discrepancy of the results among the latter three cases is small, but it seems to be due to the effect of the inlet flow conditions which is related to thickness of the boundary layer at entrance of the bend. Such effect was also observed by Govindan et al.[20].

Figure 2 shows the streamwise velocity profiles by Case I compared with experiments[2] at the several streamwise stations of the X-Z symmetry plane. The comparison is quite satisfactory except near

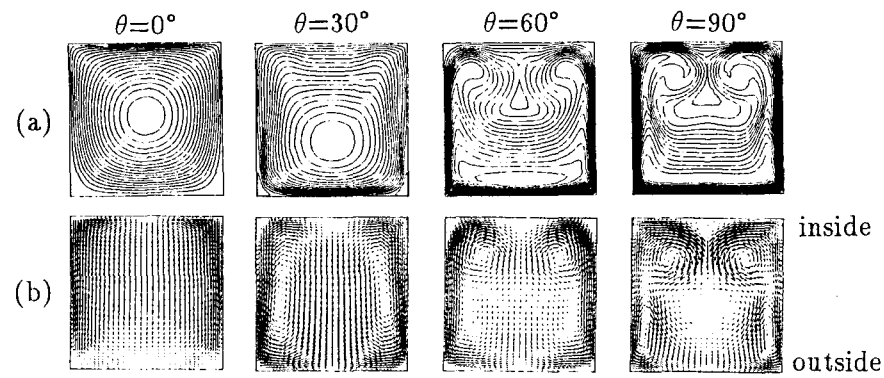

Fig.3 Computational results of (a) streamwise velocity contours and (b) secondary velocity vectors on the several cross-section plane (Case I)

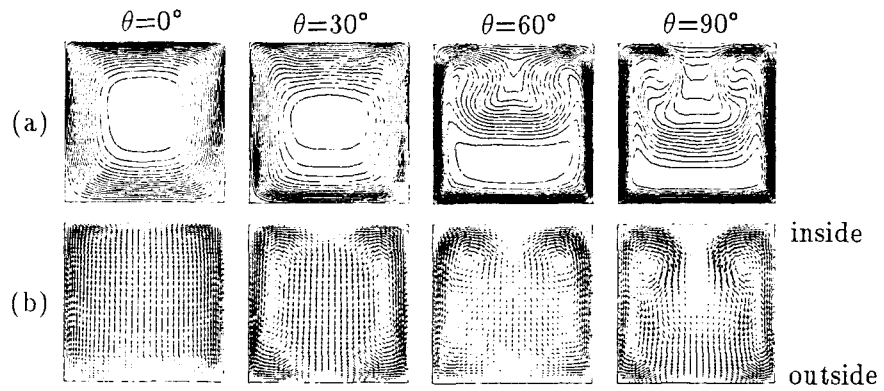

Fig.4 Computational results of (a) streamwise velocity contours and (b) secondary velocity vectors on the several cross-section plane (Case V)

the inner wall of the rear part of the bend. These discrepancies, specifically at 60° plane, are appeared in other papers[3,21], but in this computation, it is considered that the forming of the second maximum in the velocity occuring further upstream (near the θ of 50°) than that of experiments causes the discrepancy at the latter part of the bend. However, the peak velocity near the outside is very well predicted. Figures 3 and 4 show the computational results of streamwise velocity magnitude contours and secondary velocity vectors at several streamwise cross sections for the fully developed and developing entry flow case, respectively. It shows that the center of the high velocity flow moves to outer wall with the angle of θ (Fig.3(a) and 4(a)), which is due to the secondary flow formed by the curvature. Near the end of the bend, this center is shifted to both side corners of the outer wall, and the second high velocity region is formed near the inner wall. Recirculation zone exists at both corners of outside wall near 30° plane in Fig.3. On the other hand, the secondary vortices are formed at the both sides from the center of the duct, and they are seen

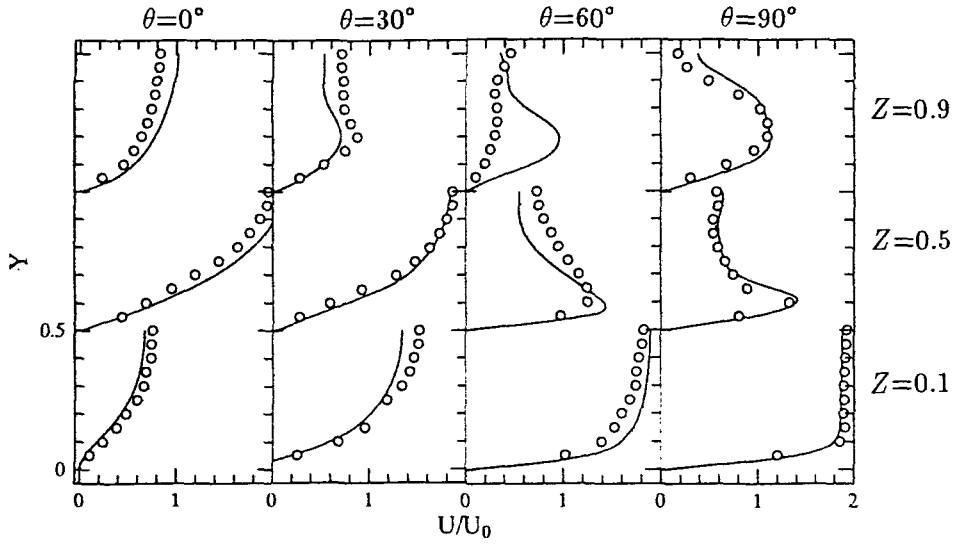

Fig.5 Streamwise velocity profiles: —, Case I; ○, Experiments[2]

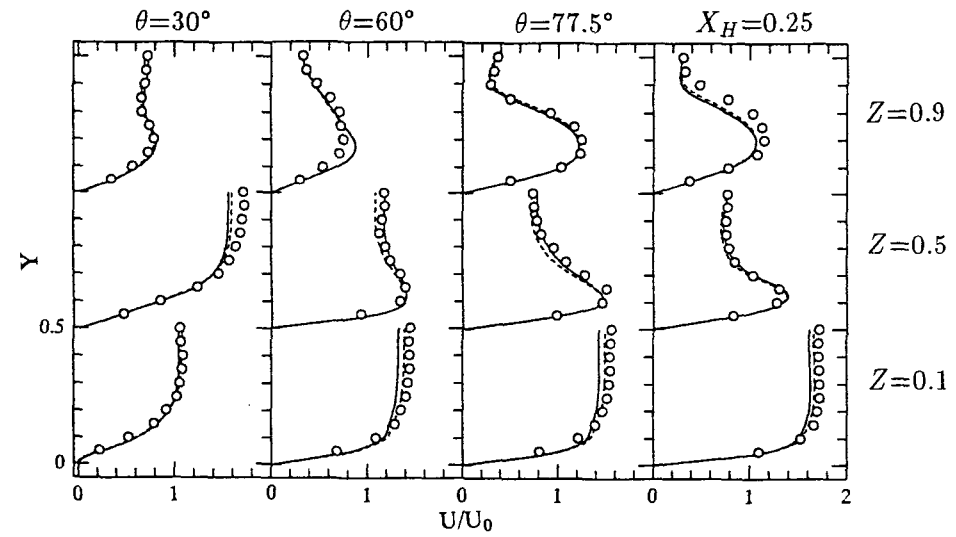

Fig.6 Streamwise velocity profiles: —, Case III; ---, Case V; ○, Experiments[5]

to become stronger and move toward the inside wall. And then, this flow develops to a very complicated secondary flow having three different vortices at 90° plane in Fig.3. These vortices are also observed near X_H=0.25 in the developing flow case.

Figures 5 and 6 show a comparison of streamwise velocity profiles along the Y lines with experiments[2,5]. The agreement between predictions and measurements is quite good at most locations. And the Case V predicts better than Case III and IV in Fig.6. Figure 7 compares the predicted secondary velocity w with experiments[5] in Case V. The present computations well capture the peak value of w

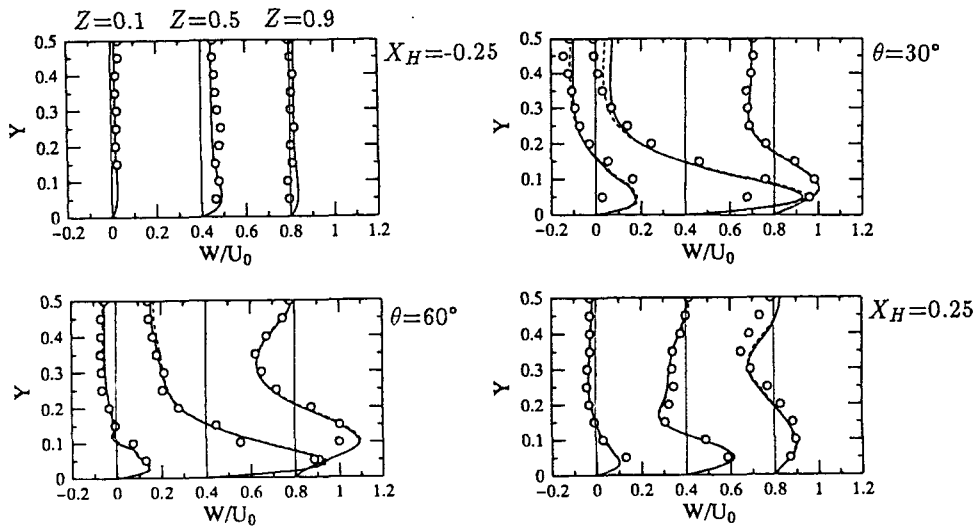

Fig.7 Secondary velocity profiles: —, Case III; ---, Case V; ○, Experiments[5]

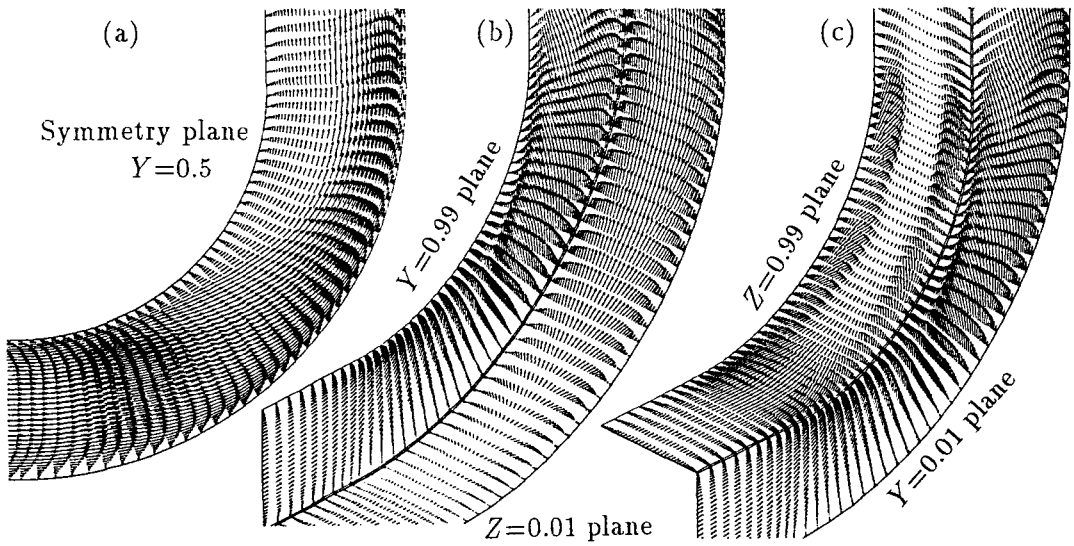

Fig.8 Streamwise velocity vectors (Case V)

and all the qualitative features of the flow. Figures 8(a)-(c) show streamwise velocity vectors on the symmetry plane (Y=0.5), on the left hand side wall (Y=0.99) and outer wall (Z=0.01), and on the inner wall (Z=0.99) and the right hand side wall (Y=0.01). Redistributions of the velocity along the streamwise direction and the recirculation zone which is formed at both side corners of the outside wall near 5°~40° are seen in this figure. The second maximum velocity occurs near 50°. And the double peak of the velocity profile exists near inner wall of the bend region.

Figures 9(a)-(c) show the streamlines along the bend and the vorticity magni-

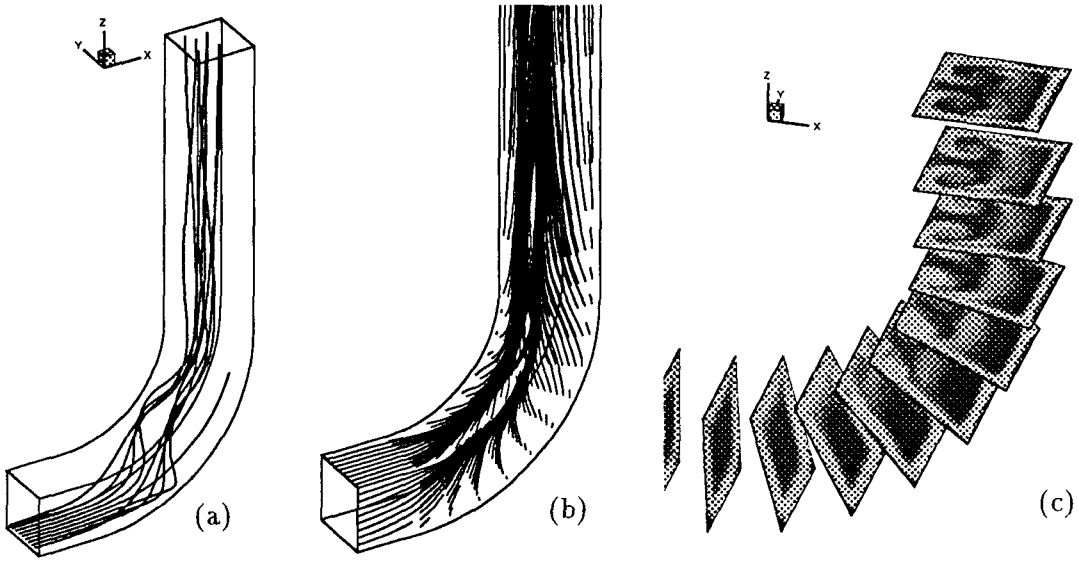

Fig.9 Numerical results of (a) streamlines, (b) oil flow patterns and (c) vorticity magnitude contours (Case V)

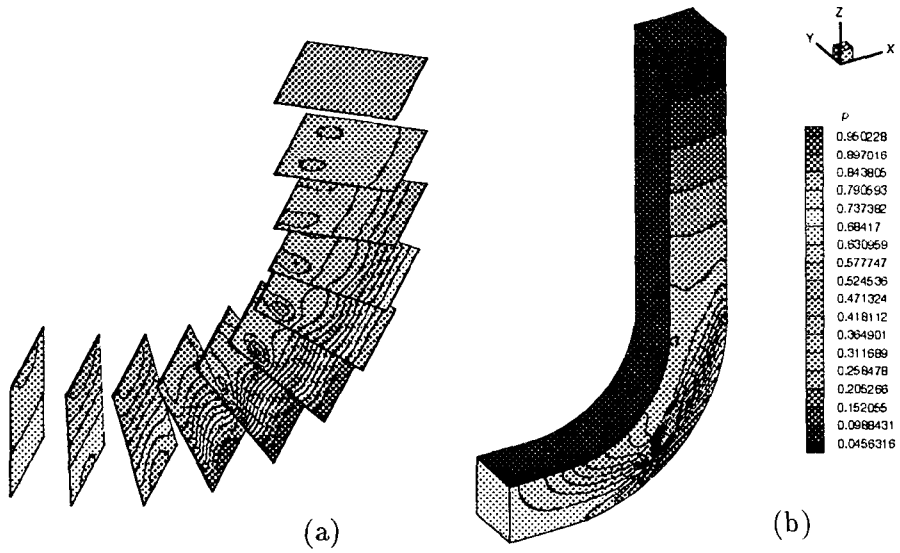

Fig.10 Numerical results of (a) pressure contours and (b) surface pressure distributions (Case V)

tude contours at several streamwise cross sections by the 3-D computer graphics. The vortex pair originated at beginning of the bend is observed. Also, the separation region can be seen in Fig.9(b) of the oil flow pattern on the inside wall. Figure 10 shows the numerical results of pressure contours and the surface pressure distribution. In the bended area, relatively high pressure are distributed near the outside wall because of the centrifugal forces. At downstream from the bend, the pressure is

recovered to the uniform value across the cross-section.

5. Conclusions

An incompressible developing and fully developed entry flow through a square duct with a 90 degree bend is studied numerically by using an efficient implicit SMAC scheme, which was developed previously for solving the 3-D Navier-Stokes equations in general curvilinear coordinates. In the present computation, 3-D complex flow phenomena including strong secondary motion in the curved duct are simulated well, so that it is easy to understand that kind of flow behavior and makes possible to take a sufficient information required for efficient designs of fluid devices. Also, a good agreement with experimental data is obtained. It indicates that the present scheme is a high reliability for computing the square duct or similar duct with a strong curvature to be basic physical elements associated with turbomachinery.

References

[1] Akiyama, M., Hanaoka, Y. and Cheng, K. C., (1984) "A Study of Laminar Flow in the Entrance Region of Curved Popes," *JSME Ser. B*, **50**-449, p.286.

[2] Humphrey, J. A. C., Taylor, A. M. K. and Whitelaw, J. H., (1977) "Laminar Flow in a Square Duct of Strong Curvature," *J. Fluid. Mech.*, **83**, Part 3, p.509.

[3] Sotirpoulos, F., Kim, W. J. and Patel, V. C., (1994) "A Computational Comparision of Two Incompressible Navier-Stokes Solvers in Three-Dimensional Laminar Flows," *Computers Fluids*, **23**-4, p.627.

[4] Cabuk, H., Sung, C. H. and Modi, V., (1992) "Explicit Runge-Kutta Method for Three-Dimensional Internal Incompressible Flows," *AIAA J.*, **30**-8, p.2024.

[5] Taylor, A.M.K., Whitelaw, J. H. and Yianneskis, M., (1982) "Curved Ducts with Strong Secondary Motion: Velocity Measurements of Developing Laminar and Turbulent Flow," *ASME J. Fluid Eng.*, **104**-9, p.350.

[6] Hallow, F. H. and Welch, J. E., (1965) "Numerical Calculation of Time Dependent Viscous Incompressible Flow of Fluid with Free Surface," *Phys. Fluids*, **8**-12, p.2182.

[7] Amsden, A. A. and Harlow, F. H., (1970) "A Simplified MAC Technique for Incompressible Fluid Flow Calculations," *J. Comput. Phys.*, **6**-2, p.322.

[8] Kim, J. and Moin, P., (1985) "Application of a Fractional-Step Method to Incompressible Navier-Stokes Equation," *J. Comput. Phys.*, **59**-2, p.308.

[9] Chorin, A. J., (1967) "Numerical Method for Solving Incompressible Viscous Flow Problems," *J. Comput. Phys.*, **2**-1, p.12.

[10] Chang, J.L.C., Kwak, D., Rogers, S. E. and Yang, R. J., (1988) "Numerical Simulation Methods of Incompressible Flows and an Application to the Space Shuttle Main Engine," *Int. J. Num. Meth. Fluids*, **8**-10, p. 1241.

[11] Rosenfeld, M., Kwak, D. and Vinokur, M., (1991) "A Fractional Step Solution Method for the Unsteady Incompressible Navier-Stokes Equations in Generalized Coordinate Systems," *J. Comput. Phys.*, **94**-1, p.102.

[12] Ikohagi, T., Shin, B. R. and Daiguji, H., (1992) "Application of an Implicit Time-marching Scheme to 3-D Incompressible Flow Problem in Curvilinear Coordinate Systems," *Computers Fluids*, **21**-2, p.163.

[13] Shin, B.R., Ikohagi, T. and Daiguji,

H., (1993) "A Finite Difference Scheme for the Two Dimensional Incompressible Turbulent Flows Using Curvilinear Coordinates," *JSME Int'l J.*, Ser. B, **36**-4, p.607.

[14] Beam, R. M. and Warming, R. F., (1978) "An Implicit Factored Scheme for the Compressible Navier-Stokes Equations," *AIAA J.*, **16**-4, p.393.

[15] Hirt, C. W., Nichols, B. D, and Romero, R., (1975) "SOLA-A Numerical Solution Algorithm for Transient Fluid Flows," Los Alamos Scientific Lab. Rep. LA-5852.

[16] Patankar, S. V. and Spalding, D. B. (1972) "A Calculation Procedure for Heat, Mass and Monentum Transfer in Three-dimensional Parabolic Flows," *Int. J. Heat Mass Transfer*, **15**, p.1787.

[17] Shin, B. R., Ikohagi, T. and Daiguji, H., (1995) "An Implicit Finite Difference Scheme for the Incompressible Navier-Stokes Equations Using an Improved Factored Scheme," *Comput. Fluid Dyn. J.*, 4-2, p.191.

[18] Chakravarthy, S. R. and Osher, S., (1985) "A New Class of High Accuracy TVD Schemes for Hyperbolic Conservation Laws," *AIAA Paper* 85-0363.

[19] White, F. M., (1974) "Viscous Fluid Flow," McGraw-Hill, New York, p.123.

[20] Govindan, T. R., Briley, W. R. and McDonald, H., (1991) "General Three Dimensional Viscous Primary / Secondary Flow Analysis," *AIAA J.*, **29**-3, p.361.

[21] Yeo, R. W., Wood, P. E. and Hrymak, A. N., (1991) "A Numerical Study of Laminar 90-Degree Bend Duct Flow with Different Discretization Schemes," *ASME J. Fluid Eng.*, **113**-12, p.563.